Journal of Inorganic Biochemistry 260 (2024) 112691

Contents lists available at ScienceDirect

Journal of Inorganic Biochemistry

journal homepage: www.elsevier.com/locate/jinorgbio

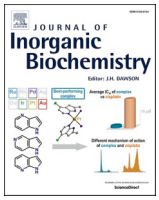

Kinetic and structural analysis of redox-reversible artificial imine reductases

Alex H. Miller [a], Ingrid B.S. Martins [b,c], Elena V. Blagova [d], Keith S. Wilson [d], Anne-K. Duhme-Klair [a,*]

[a] Department of Chemistry, University of York, Heslington, York YO10 5DD, United Kingdom
[b] Department of Physics, Institute of Biosciences, Humanities and Exact Sciences, São Paulo State University (UNESP), São José do Rio Preto, SP 15054-000, Brazil
[c] Biophysics Institute Carlos Chagas Filho, Federal University of Rio de Janeiro, Rio de Janeiro, RJ 21941-902, Brazil
[d] Structural Biology Laboratory, Department of Chemistry, University of York, Heslington, York YO10 5DD, United Kingdom

ARTICLE INFO

Keywords:
Artificial metalloenzymes
Michaelis-Menten
Kinetics
Molecular docking

ABSTRACT

Three artificial imine reductases, constructed *via* supramolecular anchoring utilising Fe^{III}-azotochelin, a natural siderophore, to bind an iridium-containing catalyst to periplasmic siderophore-binding protein (PBP) scaffolds, have previously been synthesised and subjected to catalytic testing. Despite exhibiting high homology and possessing conserved siderophore anchor coordinating residues, the three artificial metalloenzymes (ArMs) displayed significant variability in turnover frequencies (TOFs). To further understand the catalytic properties of these ArMs, their kinetic behaviour was evaluated with respect to the reduction of three cyclic imines: dihydroisoquinoline, harmaline, and papaverine. Kinetic analyses revealed that all examined ArMs adhere to Michaelis-Menten kinetics, with the most pronounced saturation profile observed for the substrate harmaline. Additionally, molecular docking studies suggested varied hydrogen-bonding interactions between substrates and residues within the artificial binding pocket. Pi-stacking and pi-cation interactions were identified for harmaline and papaverine, corroborating the higher affinity of these substrates for the ArMs in comparison to dihydroisoquinoline. Furthermore, it was demonstrated that multiple cavities are capable of accommodating substrates in close proximity to the catalytic centre, thereby rationalising the moderate enantioselectivity conferred by the unmodified scaffolds.

1. Introduction

Artificial metalloenzyme (ArM) development represents a versatile strategy that merges the benefits of protein scaffolds with tailor-made synthetic catalysts [1–7]. The effectiveness of a metalloenzyme's catalytic function depends on both the immediate coordination environment of the metal ion and the protein framework enveloping it [1,8]. By integrating non-natural metal centres or cofactors into native protein structures, researchers aim to create artificial metalloenzymes capable of emulating the functionalities of natural metalloenzymes. Notably, protein scaffolds can not only enhance the solvent tolerance of inorganic catalysts *via* the secondary coordination sphere [4,9], but also improve (*enantio*)selectivity by directing the substrate orientation within engineered binding sites [1,5].

Our research group devised an ArM using a supramolecular anchoring strategy [2]. An iron-siderophore anchor (Fe^{III}-azotochelin) was utilised to bind an iridium-containing catalyst as abiological cofactor, [Fe^{III}(**1**)Cp*Ir^{III}], Fig. 1a. The siderophore-anchored cofactor exhibited nanomolar affinity for a periplasmic binding protein from *Campylobacter jejuni,* ***Cj***CeuE. The crystal structure of the resulting artificial metalloenzyme [Fe^{III}(**1**)Cp*Ir^{III}] ⊂ ***Cj***CeuE (PDB: 5DO5_1) is shown in Fig. 1b. This ArM displayed imine reductase activity towards a model substrate, 6,7-dimethoxy-1-methyl-3,4-dihydroisoquinoline (**2**, referred to as **dihydroisoquinoline**), Fig. 1c, achieving around 33% enantiomeric excess (e.e.) without any scaffold optimisation, however, only a low turnover frequency (TOF) of 0.30 min^{-1} was obtained. Subsequently, we identified two potential homologues of ***Cj***CeuE from thermophilic organisms, *Geobacillus stearothermophilus*, ***Gst***CeuE, and *Parageobacillus thermoglucosidasius*, ***Pth***CeuE, [10] which enabled the development of the ArMs [Fe^{III}(**1**)Cp*Ir^{III}] ⊂ ***Gst***CeuE and [Fe^{III}(**1**)Cp*Ir^{III}] ⊂ ***Pth***CeuE. These ArMs exhibited improved TOFs of around 1.71 min^{-1} [3], albeit with slightly reduced e.e. for the

* Corresponding author.
E-mail address: anne.duhme-klair@york.ac.uk (A.-K. Duhme-Klair).

https://doi.org/10.1016/j.jinorgbio.2024.112691
Received 10 June 2024; Received in revised form 29 July 2024; Accepted 4 August 2024
Available online 6 August 2024

dihydroisoquinoline model substrate (29 and 24%, respectively). Both homologues have conserved anchor-binding residues and exhibit very similar folded structures (Fig. 1b).

Whilst the crystal structures of ***Gst***CeuE and ***Pth***CeuE with the bound azotochelin anchor could be determined, crystallising the respective ArMs proved challenging and was unsuccessful. Comparing the structures of the artificial imine reductase [Fe^{III}(**1**)Cp*Ir^{III}] ⊂ ***Cj***CeuE with those of Fe^{III}-azotochelin⊂***Gst***CeuE (PDB: 8bax) and Fe^{III}-azotochelin⊂***Pth***CeuE (PDB: 8bf6) revealed a similar position of the anchor moiety among the three structures (Fig. 1b, insert). However, these findings did not shed light on the exact position and orientation of the catalytic moiety. Computational approaches could aid in predicting favourable positions of the cofactor, although molecular modelling of ArMs presents challenges due to their multiple components: protein scaffold, cofactor, substrates, and interactions between metal species and proteins [5].

Having established the catalytic activity of the three ArMs, we were interested in investigating whether these ArMs exhibit kinetics akin to natural enzymes. Whilst ArMs have previously been reported to display enzyme-like kinetics (Michaelis-Menten saturation) [1,7,11,12], some studies have indicated deviations, with certain ArMs failing to demonstrate conventional saturation kinetics [12–14]. To gain further structural and kinetic insights that could aid in enhancing ArM selectivity, we selected two additional cyclic imines as model substrates for our kinetic studies: 1-methyl-7-methoxy-3,4-dihydro-beta-carboline (**4**, referred to as **harmaline**, Fig. 1d), previously tested utilising immobilised [Fe^{III}(**1**)Cp*Ir^{III}] ⊂ ***Gst***CeuE [3,15], and 1-[(3,4-dimethoxyphenyl)methyl]-3,4-dihydro-6,7-dimethoxyisoquinoline (**6**, referred to as **papaverine**, Fig. 1e), both were tested in parallel with **2**. Additionally, molecular docking studies were performed to model substrate binding to the catalytic site of these enzymes.

2. Results and discussion

2.1. Substrate specificity

To survey the substrate specificity of the artificial imine reductases described herein, they were challenged with a selection of model substrates. Two cyclic imines (**4** and **6**) with structures that differ significantly from that of substrate **2**, were chosen. The dihydro-beta-carboline derivative **4**, is slightly larger than **2** and lacks one of the OMe-based hydrogen bond acceptors whilst containing an additional hydrogen bond donor (NH). Substrate **6** on the other hand, is a sterically more demanding derivative of **2** that contains two additional OMe-based hydrogen-bond acceptors. Reaction rates were monitored by following the decrease in the intensity of the imine absorption band at 375 nm for **4** and at 350 nm for both **2** and **6** [3]. Reactions performed with 50 mM concentrations of **2** were previously reported [2,3] and the results are presented in Table 1, entries 1–3, for reference. Due to the lower solubility of **4** and **6** in the catalytic buffer, the reaction conditions had to be slightly adjusted, and a substrate concentration of 10 mM was used instead. Additionally, the pH of the buffer was increased from 6 to 7. Control experiments using a 10 mM concentration of **2** at pH 7 were therefore performed, using both unbound catalyst [Fe^{III}(**1**)Cp*Ir^{III}] and the [Fe^{III}(**1**)Cp*Ir^{III}] ⊂ ***Gst***CeuE ArM for comparison (Table 1, entries 4 and 5). The change in reaction conditions caused a decrease in TOF from 1.71 min^{-1} to 1.10 min^{-1} and a decrease in the e.e. from 29 to 12% for [Fe^{III}(**1**)Cp*Ir^{III}] ⊂ ***Gst***CeuE (Table 1, entries 2 and 4). All further tests were run at 10 mM substrate and pH 7 to facilitate comparison.

[Fe^{III}(**1**)Cp*Ir^{III}], [Fe^{III}(**1**)Cp*Ir^{III}] ⊂ ***Cj***CeuE, [Fe^{III}(**1**)Cp*Ir^{III}] ⊂ ***Gst***CeuE and [Fe^{III}(**1**)Cp*Ir^{III}] ⊂ ***Pth***CeuE displayed similar trends for the reduction of **2**, **4** and **6** (Table 1). As expected, racemic amine products were obtained with unbound catalyst cofactor [Fe^{III}(**1**)Cp*Ir^{III}]. Interestingly, faster reaction rates were achieved with the more thermostable homologues [Fe^{III}(**1**)Cp*Ir^{III}] ⊂ ***Gst***CeuE and [Fe^{III}(**1**)Cp*Ir^{III}] ⊂ ***Pth***CeuE if compared to [Fe^{III}(1)Cp*Ir^{III}] ⊂ ***Cj***CeuE. Unexpectedly, the sterically-demanding 4-ethyl-1,2-dimethoxybenzene moiety in **6** did not

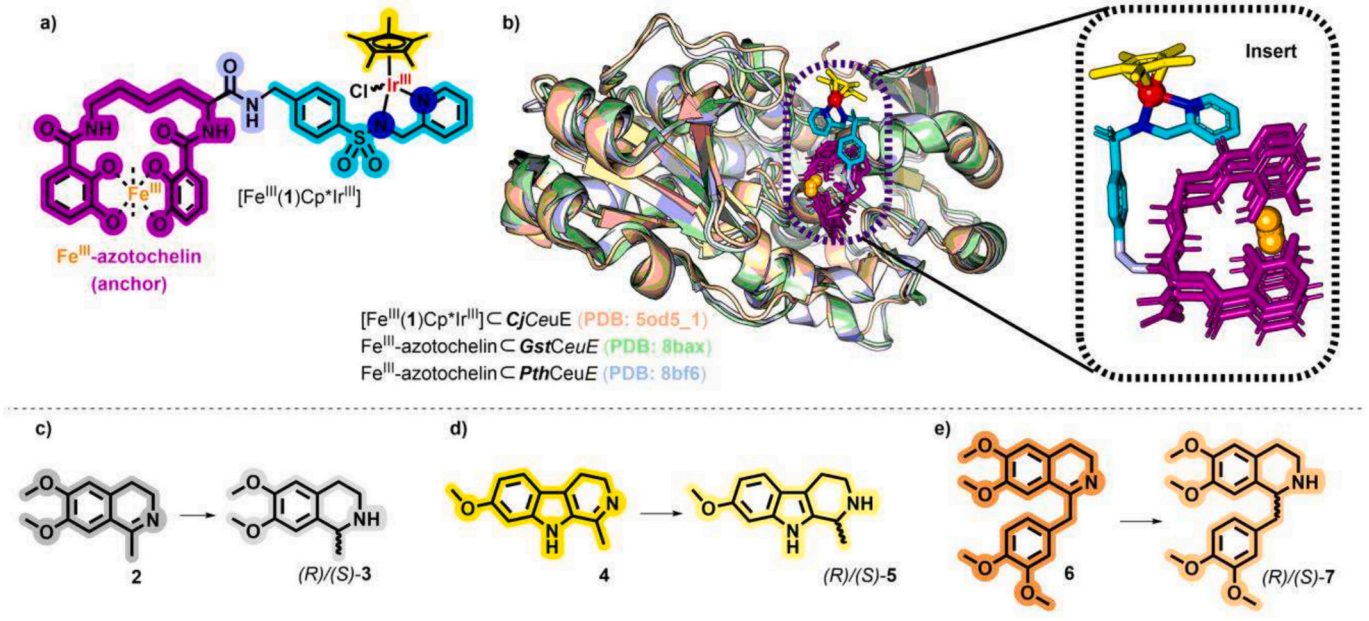

Fig. 1. Representation of cofactor and ArM or scaffolds/anchor crystal structures. **a)** Catalytic cofactor: specific coloration to denote different components: iridium (red), iron (orange), azotochelin moiety (purple), pyridinesulfonamide moiety (cyan) with coordinating nitrogens (blue), and Cp* (yellow). **b)** Visualisation of [Fe^{III}(**1**)Cp*Ir^{III}] ⊂ ***Cj***CeuE ArM (wheat) aligned with Fe^{III}-azotochelin⊂***Gst***CeuE (pale green) and Fe^{III}-azotochelin⊂***Pth***CeuE (light blue) in PyMol. Ligands are depicted as sticks and coloured according to the scheme in part **a**. See insert for details of ligands alignment (rotation: 180°). **c)** Molecular structure of imine substrates and their respective reduction products (chiral amines). Imines: dihydroisoquinoline (**2**), harmaline (**4**) and papaverine (**6**); Amines: (*R*)/(*S*)-salsolidine (**3**), (*R*)/(*S*)-tetrahydroharmine (**5**) and (*R*)/(*S*)-tetrahydropapaverine (**7**). (For interpretation of the references to colour in this figure legend, the reader is referred to the web version of this article.)

Table 1
Catalytic activity of [Fe^{III}(**1**)Cp^*Ir^{III}], [Fe^{III}(**1**)Cp^*Ir^{III}] ⊂ ***Cj***CeuE, [Fe^{III}(**1**)Cp^*Ir^{III}] ⊂ ***Gst***CeuE, [Fe^{III}(**1**)Cp^*Ir^{III}] ⊂ ***Pth***CeuE for the reduction of substrates **2**, **4** and **6**.

Entry	Substrate	Catalyst	Time to completion (h)	TON at completion/ TOF (min^{-1})	*(R)* e.e. %	*Ref.*
1	**2**	[Fe^{III}(**1**)Cp^*Ir^{III}] ⊂ ***Cj***CeuE	24[#]	400 / 0.30[a]	35	[2]
2		[Fe^{III}(**1**)Cp^*Ir^{III}] ⊂ ***Gst***CeuE	7[#]	400 / 1.71[b]	29	[3]
3		[Fe^{III}(**1**)Cp^*Ir^{III}] ⊂ ***Pth***CeuE	7[#]	400 / 1.71[b]	24	
4		[Fe^{III}(**1**)Cp^*Ir^{III}	1[&]	200 / 3.33[c]	<3	This work
5		[Fe^{III}(**1**)Cp^*Ir^{III}] ⊂ ***Gst***CeuE	5[&]	200 / 1.10[c]	12	
6	**4**	[Fe^{III}(**1**)Cp^*Ir^{III}	1[&]	200 / 3.33[c]	<3	
7		[Fe^{III}(**1**)Cp^*Ir^{III}] ⊂ ***Cj***CeuE	24[&]	200 / 0.55[c]	29	
8		[Fe^{III}(**1**)Cp^*Ir^{III}] ⊂ ***Gst***CeuE	3[&]	200 / 1.93[c]	31	
9		[Fe^{III}(**1**)Cp^*Ir^{III}] ⊂ ***Pth***CeuE	4[&]	200 / 1.53[c]	20	
10	**6**	[Fe^{III}(**1**)Cp^*Ir^{III}	1[&]	200 / 3.33[c]	<3	
11		[Fe^{III}(**1**)Cp^*Ir^{III}] ⊂ ***Cj***CeuE	24[&]	200 / 0.56[c]	35	
12		[Fe^{III}(**1**)Cp^*Ir^{III}] ⊂ ***Gst***CeuE	3[&]	200 / 2.57[c]	28	
13		[Fe^{III}(**1**)Cp^*Ir^{III}] ⊂ ***Pth***CeuE	3[&]	200 / 2.10[c]	19	

[#] Reaction conditions: 50 mM substrate / 0.125 mM catalyst / 40 °C / 400 rpm / pH 6.
[&] Reactions conditions:10 mM substrate / 0.05 mM catalyst / 45 °C / 400 rpm / pH 7.
[a] TOF calculated at 8 h. [b] TOF calculated at 3 h. [c] TOF calculated at 1 h.

induce significant changes in the enantioselectivity achieved by the three artificial imine reductases when compared with substrates **2** and **4**. The e.e. values achieved in the reduction of substrates **2, 4** and **6** by [Fe^{III}(1)Cp^*Ir^{III}] ⊂ ***Gst***CeuE differ significantly, with the formation of *(R)*-**3**, *(R)*-**5** and *(R)*-**7** proceeding with e.e. values of 12, 31 and 28%, respectively (Table 1, entries 5, 8 and 12). Although only relatively subtle, the changes in both reactivity and selectivity observed with the different substrates highlight the benefits of introducing a protein scaffold that imparts a second-sphere coordination environment to an inorganic cofactor [16–18], and enables substrate interactions that resemble those found in the binding pockets of natural enzymes. We have previously reported that a histidine residue (His227), which coordinates to the iridium centre in [Fe^{III}(1)Cp^*Ir^{III}] ⊂ ***Cj***CeuE, plays a key role in conferring enantioselectivity, albeit at the cost of the TOF [2] and note that this histidine residue is conserved in both ***Gst***CeuE and ***Pth***CeuE [3,10]. The replacement of histidine with alanine resulted in a [Fe^{III}(**3**)Cp^*Ir^{III}] ⊂ ***Cj***H227A variant with negligible enantioselectivity and significantly higher TOF [2]. Therefore, we anticipate that an in-depth understanding of the structure and dynamics of these ArMs will be crucial for their optimisation.

2.2. Michaelis-Menten kinetics for substrates 2, 4 and 6

Michaelis-Menten kinetic investigations provided valuable insights into the interactions between the artificial imine reductases studied herein and imines **2, 4** and **6**, culminating in the formation of the respective *(R)/(S)*-amines (Fig. 2, Table 2). The kinetic measurements were carried out in 96-well plates, which required concentrations to be lowered (3 μM ArM, <0.6 mM substrate) to accelerate data collection whilst keeping the UV/vis absorbance used to follow reaction progress within a quantifiable range.

Saturation curves were obtained for each ArM/substrate pair (Fig. 2), confirming that the artificial imine reductases show Michaelis-Menten-type behaviour and that there are significant interactions between the protein binding pockets and the chosen substrates. A negative control experiment with [Fe^{III}(**1**)Cp^*Ir^{III}] was conducted, and as expected typical Michaelis-Menten-type behaviour was not observed (**Fig. S1**).

The analysis of the K_m values obtained revealed a consistent trend among the three artificial imine reductases, with the highest affinity observed for substrate **4**, followed by **6** and then **2**. This observation suggests that the additional NH group provided by the dihydro-beta-carboline derivative **4** (harmaline) donates a hydrogen bond that contributes significantly to the binding of this substrate, which is expected considering the influence of non-covalent interactions in the specificity and stereoselectivity of natural and artificial metalloenzymes [19–21]. Substrate **6** contains two additional OMe-based hydrogen-bond acceptors that also gave rise to an enhanced binding affinity. It is worth noting that the k_{cat} values obtained with the ***Cj***CeuE- ***Gst***CeuE- and ***Pth***CeuE-based ArMs (Table 2) are more similar than the corresponding concentration-dependent TOFs (Table 1), which suggests that the ***Cj***CeuE-based ArM performs comparatively better in dilute solutions, as used in the Michaelis Menten kinetic studies. In this context, it is important to highlight a number of extra challenges in our system: the potential dissociation of the artificial cofactor [Fe^{III}(**1**)Cp^*Ir^{III}] from the protein, catalyst decomposition due to iridium dissociation from ligand **1** and the inability to monitor the binding status in real time.

The ArM concentrations used were more than two orders of magnitude above the dissociation constants of their respective siderophore-based anchoring units (23, 9 and 18 nM for the ***Cj***CeuE-, ***Gst***CeuE- and ***Pth***CeuE-ArMs, respectively [3]), and hence inflated catalytic rates caused by significant amounts of dissociated catalytic cofactor are unlikely. Since the free artificial cofactor gives rise to high TOFs, but does not exhibit Michaelis-Menten-type behaviour (**Fig. S1**), the saturation curves obtained with the three ArMs (Fig. 2) support this assertion.

It is conceivable, however, that upon dilution some of the iridium dissociates from ligand **1**, and that the fractional iridium occupancy remains most favourable in case of the ***Cj***CeuE-ArM, potentially due to the dual iridium anchoring *via* **1** and His227 coordination, which was observed in the crystal structure of [Fe^{III}(**1**)Cp^*Ir^{III}] ⊂ ***Cj***CeuE. Interestingly, the conversion of the lower-affinity substrates **2** and **6** is more affected than that of the more strongly bound **4**, which may point towards stabilising interactions of **4** with both the Ir-catalyst and the respective protein binding pockets of the ***Gst***- and ***Pth***-ArMs. Since the crystal structures of the latter have not yet been determined, future investigations will be aimed at exploring this dual anchoring hypothesis further.

The catalytic efficiencies (k_{cat}/K_m) for substrates **2** and **6** were also similar across the three artificial imine reductases, except for [Fe^{III}(**1**)Cp^*Ir^{III}] ⊂ ***Pth***CeuE, which displayed a slightly lower efficiency. [Fe^{III}(**1**)Cp^*Ir^{III}] ⊂ ***Gst***CeuE exhibited the highest affinity for substrate **4** and the most favourable overall catalytic efficiency for the formation of *(R)/(S)*-**5**. Whilst this catalytic efficiency approaches that of some natural imine reductases reported in the literature [22], most naturally-evolved

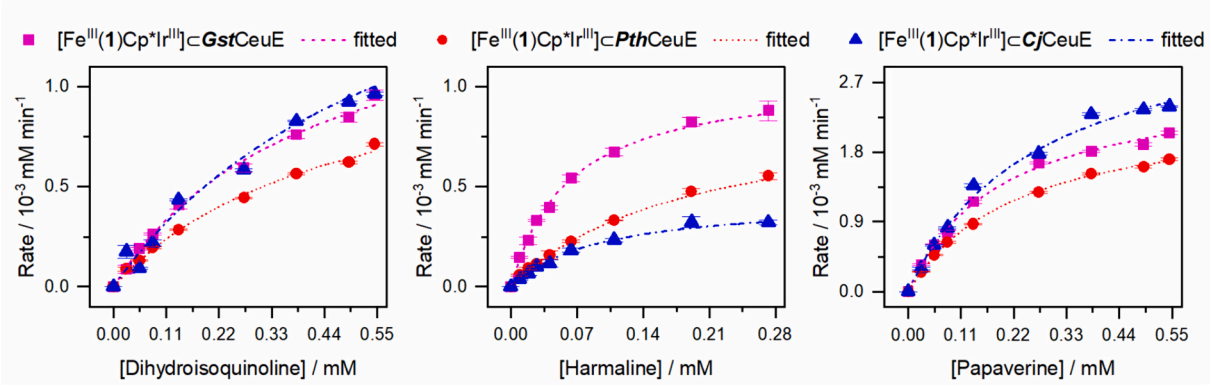

Fig. 2. Michaelis-Menten Plots: Rate *vs.* substrate concentration curves for the ArMs for three different substrates (harmaline, dihydroisoquinoline, papaverine). Fitted curves are shown as dotted, dashed or dashed-dotted lines. $R^2 > 0.99$ in all cases. Technical triplicates. Data obtained with the free unbound catalyst did not follow Michaelis-Menten kinetics and the data could not be fitted (**Fig. S1**).

Table 2
Michaelis-Menten parameters for the reduction of substrates **2**, **4** and **6** by the artificial imine reductases.

Substrate	ATHase[1]	K_m (mM)	V_{max} (10^{-3} mM min^{-1})	k_{cat} (min^{-1})	k_{cat}/K_m (min^{-1} mM^{-1})
2	[Fe^{III}(**1**)Cp*Ir^{III}] ⊂ ***Gst***CeuE	0.42 ± 0.03	1.61 ± 0.07	0.54 ± 0.02	1.3 ± 0.1
	[Fe^{III}(**1**)Cp*Ir^{III}] ⊂ ***Pth***CeuE	0.48 ± 0.05	1.26 ± 0.08	0.42 ± 0.03	0.9 ± 0.1
	[Fe^{III}(**1**)Cp*Ir^{III}] ⊂ ***Cj***CeuE	0.6 ± 0.2	2.2 ± 0.5	0.7 ± 0.2	1.1 ± 0.5
4	[Fe^{III}(**1**)Cp*Ir^{III}] ⊂ ***Gst***CeuE	0.062 ± 0.005	1.06 ± 0.05	0.35 ± 0.02	5.7 ± 0.5
	[Fe^{III}(**1**)Cp*Ir^{III}] ⊂ ***Pth***CeuE	0.19 ± 0.03	0.91 ± 0.08	0.3 ± 0.03	1.6 ± 0.3
	[Fe^{III}(**1**)Cp*Ir^{III}] ⊂ ***Cj***CeuE	0.095 ± 0.007	0.44 ± 0.02	0.146 ± 0.005	1.5 ± 0.1
6	[Fe^{III}(**1**)Cp*Ir^{III}] ⊂ ***Gst***CeuE	0.19 ± 0.01	2.75 ± 0.07	0.92 ± 0.02	4.7 ± 0.3
	[Fe^{III}(**1**)Cp*Ir^{III}] ⊂ ***Pth***CeuE	0.230 ± 0.008	2.40 ± 0.04	0.80 ± 0.01	3.5 ± 0.1
	[Fe^{III}(**1**)Cp*Ir^{III}] ⊂ ***Cj***CeuE	0.27 ± 0.03	3.7 ± 0.2	1.23 ± 0.06	4.5 ± 0.5

[1] Reaction conditions: Fixed: 3 μM ATHase concentration, 220 μl total reaction volume, 0.6 M MES / 3 M HCOONa / catalytic buffer at pH 7, 40 °C incubation, 600 r.p.m. shaking. Varied: substrate concentration in the range 0 to 0.6 mM.

enzymes achieve higher efficiencies. Nevertheless, it is of note that all three artificial imine reductases, namely [Fe^{III}(**1**)Cp*Ir^{III}] ⊂ ***Gst***CeuE, [Fe^{III}(**1**)Cp*Ir^{III}] ⊂ ***Pth***CeuE and [Fe^{III}(**1**)Cp*Ir^{III}] ⊂ ***Cj***CeuE, either equalled or surpassed the catalytic efficiency of a number of artificial imine reductases that had undergone directed evolution or site-directed mutagenesis to enhance their enzyme-like characteristics [11,23–25].

2.3. Molecular docking for substrates *2, 4 and 6*

Molecular docking constitutes a valuable tool in the design and optimisation of artificial metalloenzymes [7,26,27]. With the aim of elucidating the interactions between the three substrates and our ArMs, we employed this technique using the crystal structure of the [Fe^{III}(**1**)Cp*Ir^{III}] ⊂ ***Cj***CeuE to investigate favourable docking orientations of substrates within the cavities encasing the cofactor, herein referred to as the artificial binding pocket. Interestingly, using blind docking (in which the binding site is not informed), the highest scored docking conformations for all substrates were situated within the artificial binding pocket of the ArM (Fig. 3a-c). Notably, the secondary favoured pose for dihydroisoquinoline closely approximated the spatial arrangement of the primary pose, whereas the tertiary pose was displaced from the binding pocket. All docked poses are illustrated in **Fig. S2**. Pose 4 for dihydroisoquinoline (Fig. 3d) was preferentially chosen for analysis due to its proximity to the catalytic site, and occupancy of a distinct cavity than that of pose 1. The secondary favoured pose for harmaline (Fig. 3e) and papaverine (Fig. 3f) also resided within the binding pocket, albeit in distinct cavities compared to the primary poses.

Papaverine exhibited a marginally higher docking score, with harmaline and dihydroisoquinoline following closely (**Table S1**), indicating a greater biding affinity of papaverine to the ArM [28]. While this observation only partially aligns with the trends observed in the K_m values from the saturation kinetics, it is noteworthy that [Fe^{III}(**1**)Cp*Ir^{III}] ⊂ ***Cj***CeuE demonstrated the highest catalytic efficiency for papaverine (4.5 ± 0.5 min^{-1} mM^{-1}), suggesting a significant role of weak interactions. Such interactions are pivotal in the design and optimisation of ArMs, influencing the binding and unbinding of substrates at catalytic sites [21,29]. The distance between the iridium atom and the imine nitrogen and carbon in the substrates were measured (**Table S1**). The iridium-carbon distances range from 6.9 Å (harmaline, pose 2) to 9.11 Å (papaverine, pose 1), which may not be favourable to the hydride transfer required for imine reduction [30]. Whilst these distances are too long to enable a direct interaction between an Ir-bound hydride and the imine bond, similar metal-imine nitrogen distances were obtained by computational docking of nicotinamide substrates to a Rh-hydride-containing ArM [7].

This limitation could potentially be addressed by constraining distances favouring hydride transfer, as discussed by Robles et al. (2014) [24]. However, in the present study, we opted to allow all degrees of freedom to provide adequate information, as strict constraints could limit insight. Nevertheless, the absence of dynamic information regarding the cofactor hinders precise modelling of the reaction mechanism, exceeding the scope of this study's objectives.

The 2D interaction diagrams in Fig. 3 (below each respective docking pose) highlight hydrogen bonding as a crucial interaction enabling substrate accommodation within the binding pocket, thereby reinforcing the assumptions drawn from the preceding kinetic data. A prevalent occurrence involves a hydrogen bond formation between Leu137 main chain amide and OMe-based hydrogen-bond acceptors present in the substrates, observed across all three substrates. In contrast, hydrogen bonding involving Arg205 is exclusively noted for harmaline and

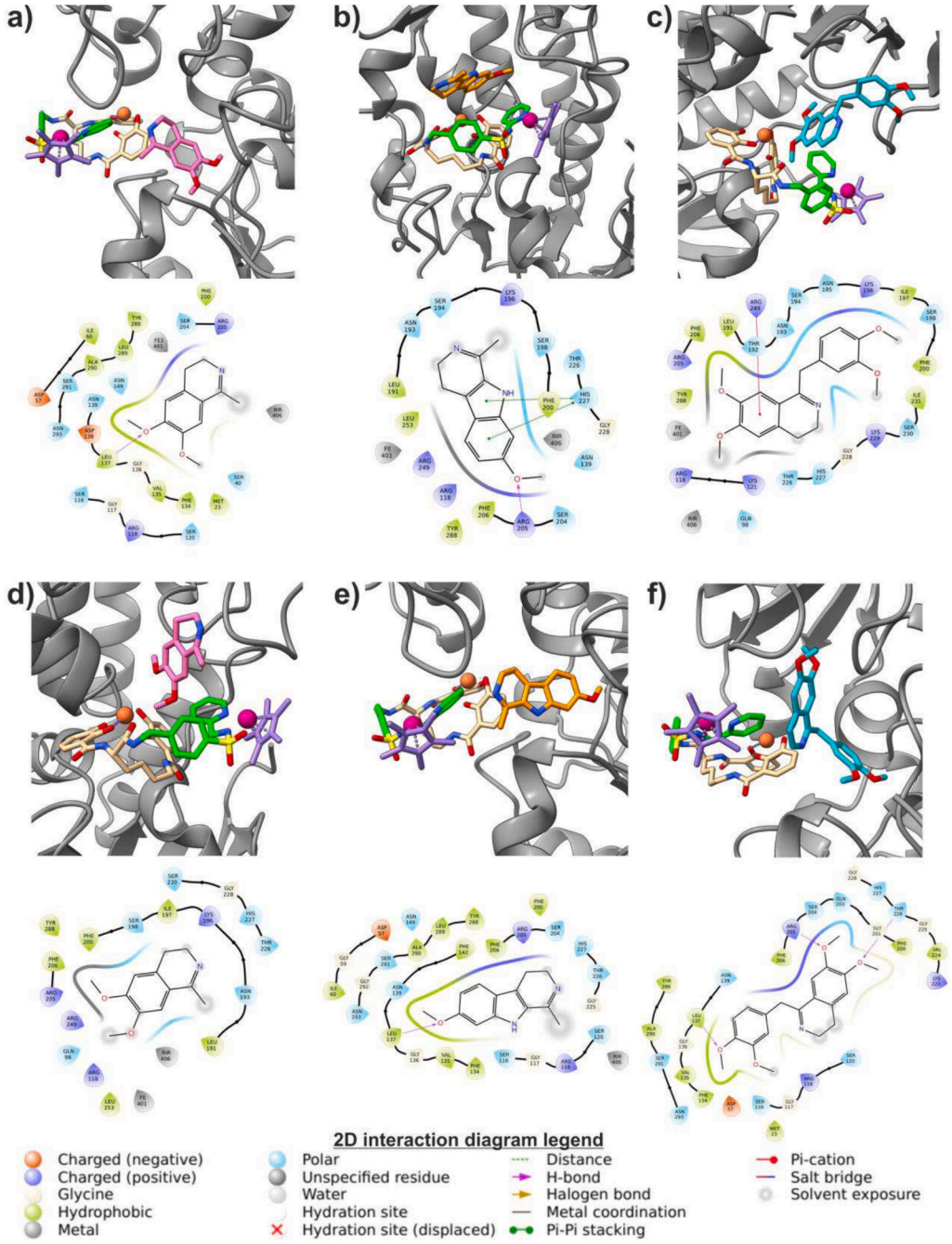

Fig. 3. Molecular docking and interaction diagrams of selected imines with the crystal structure of [Fe^{III}(**1**)Cp*Ir^{III}] ⊂ ***Cj***CeuE. Dihydroisoquinoline (magenta), harmaline (orange) and papaverine (cyan) top ranking docking poses are illustrated in **a**, **b** and **c**, respectively, as sticks. The 4th ranked pose of dihydroisoquinoline is illustrated in **d**. The 2nd ranked poses for harmaline and papaverine are illustrated in **e** and **f**, respectively. The cofactor is represented as sticks coloured in wheat, green and purple and spheres for the iron (orange) and iridium (magenta) atoms. Nitrogen atoms are coloured blue in both cofactor and substrates. 2D Interaction diagrams are provided below each docking structure (see the diagram legend at the bottom of the figure). (For interpretation of the references to colour in this figure legend, the reader is referred to the web version of this article.)

papaverine, while Thr226 demonstrates hydrogen bonding solely with papaverine. These extra hydrogen bonds could play a role in substrate binding and product release and affect the transition-state lifetimes, concomitantly enhancing or reducing enzymatic activity for different substrates. Further dynamic studies, such as molecular dynamics simulations, could be employed to explore the temporal aspects of substrate binding and unbinding, providing a more comprehensive understanding of the ArM-substrate interactions.

In addition to hydrogen bonding, a pi-stacking interaction was indicated between residue His227 and harmaline (pose 1), while a pi-cation interaction between Arg249 and papaverine (pose 1) is noted. The interaction profile suggests a higher degree of stabilising interactions for both harmaline and papaverine, which corroborates the lower K_m values (higher affinity) determined for both substrates in comparison with dihydroisoquinoline. Furthermore, the observation that all substrates can occupy multiple favourable positions within the binding pocket is to be expected, given the moderate enantioselectivity of these ArMs (below 30% e.e.).

3. Summary and conclusions

The three artificial imine reductases [Fe^{III}(**1**)Cp^*Ir^{III}] ⊂ ***Cj***CeuE, [Fe^{III}(**1**)Cp^*Ir^{III}] ⊂ ***Gst***CeuE and [Fe^{III}(**1**)Cp^*Ir^{III}] ⊂ ***Pth***CeuE exhibit Michaelis-Menten kinetics with three different imine substrates (**2**, **4** and **6**), with the highest catalytic efficiency (k_{cat}/K_m) found for the reduction of model substrate **4** (harmaline) catalysed by [Fe^{III}(**1**)Cp^*Ir^{III}] ⊂ ***Gst***CeuE. The kinetic data confirmed enzyme-like behaviour and provided evidence for a binding pocket that engages in hydrogen-bonding. The molecular docking results suggest that the PBP scaffolds are promiscuous in their current form and accommodate all three model substrates in more than one favourable position within close proximity to the cofactor. There is clear evidence for a degree of size and shape selectivity, as well as hydrogen-bonding interactions, in addition to pi-stacking and pi-cation interactions. These interactions in particular could form the basis for (stereo)selectivity improvements by site-directed or site saturation mutagenesis of hydrogen-bonding amino acid side chains in the vicinity of the binding pocket. The genetic optimisation of the PBP scaffolds will be the aim of future studies with our siderophore-anchored catalyst cofactors.

4. Materials and methods

4.1. General information

Unless otherwise noted, reagents were used as received from commercial suppliers and used as supplied. Compound **1** (**Fig. S3**), was prepared and characterised as reported [3]. The protein scaffolds were expressed and purified following our protocols [10]. The cofactor [Fe^{III}(**1**)Cp^*Ir^{III}] as well as the artificial imine reductases, [Fe^{III}(**1**)Cp^*Ir^{III}] ⊂ ***Cj***CeuE, [Fe^{III}(**1**)Cp^*Ir^{III}] ⊂ ***Gst***CeuE and [Fe^{III}(**1**)Cp^*Ir^{III}] ⊂ ***Pth***CeuE, were prepared as previously described [3]. 1-[(3,4-dimethoxyphenyl)methyl]-3,4-dihydro-6,7-dimethoxyisoquinoline was prepared following a literature procedure [31].

UV–vis spectra were recorded on a Shimadzu UV-1800 in a quartz cuvette (Starna scientific). HPLC measurements were performed on an Agilent 1200 infinity II quaternary system equipped with a 1260 Quaternary Pump G7111B, G7116A multicolumn thermostat, G7165A multiwavelength detector and G7129A Vialsampler using the specified eluent gradients. Kinetic measurements were taken at a Victor Nivo plate reader (Perkin Elmer) equipped with a 405/10 nm filter or a SpectraMax Abs+ (Molecular Devices, LLC).

4.2. Catalytic activity testing

4.2.1. Stock solutions

MES/formate buffer was prepared by dissolving 12.8 g of 2-morpholin-4-ylethanesulfonic acid monohydrate (MES monohydrate) and 20.40 g of sodium formate (HCOONa) in 80 ml water. The pH was then adjusted to 7 by addition of 5 M NaOH before the solution volume was brought up to 100 ml (final concentration 0.6 M MES, 3 M HCOONa). Stocks of dihydroisoquinoline (**2**), harmaline (**4**) and papaverine (**6**), were prepared at concentrations of 20, 12 and 20 mM, respectively, by dissolving required amounts in MES/formate buffer pH 7. Quenching solutions were prepared at concentration of 12.5 mM solution of L-glutathione in Water:MeOH (1:2) mixture, volumes as required. L-glutathione was firstly dissolved in water before addition of MeOH. Quenching solutions were stored at 4 °C and used on the day of preparation.

4.2.2. General reaction procedure for substrate screening

Reactions were carried out as previously reported, using a thermoshaker for microtubes (Grant-bio) [3]. The reactions were run in MES/formate buffer at pH 7 (0.6 M MES / 3 M HCOONa), using a 10 mM substrate concentration and 0.05 mM catalyst/ArM ([Fe^{III}(**1**)Cp^*Ir^{III}], [Fe^{III}(**1**)Cp^*Ir^{III}] ⊂ ***Cj***CeuE, [Fe^{III}(**1**)Cp^*Ir^{III}] ⊂ ***Gst***CeuE and [Fe^{III}(**1**)Cp^*Ir^{III}] ⊂ ***Pth***CeuE concentration at 45 °C and shaking speed of 400 rpm. Total volume 0.5 ml. At defined time points, 25 μl aliquots were withdrawn from the reaction mixtures and mixed with 1975 μl of the quenching solution. Total volume 0.5 ml. Quenched samples were submitted for UV–vis and chiral HPLC analysis. Chiral HPLC analysis for dihydroisoquinoline and harmaline products were carried out according to the reported methods [3]. For papaverine products, chiral separation was achieved using the same method as for harmaline products, **Fig. S4**, retention times: (*S*)-(−)-tetrahydropapaverine 14.1 min and (*R*)-(+)-tetrahydropapaverine 14.8 min.

4.3. Michaelis-Menten kinetics

The initial reaction rates of the imine reduction of **2**, **4** and **6** were evaluated in 96-well plates using a Victor Nivo plate reader (Perkin Elmer) equipped with a 405/10 nm filter (**4**) or SpectraMax Abs+ (Molecular Devices, LLC), at 380 nm (**2** and **6**). The plate was kept under 40 °C throughout the course of the reactions, and 600 rpm shaking performed in between measurements. The absorbance was collected for 100 ms. Measurements were carried out with the three ArMs ([Fe^{III}(**1**)Cp^*Ir^{III}] ⊂ ***Cj***CeuE, [Fe^{III}(**1**)Cp^*Ir^{III}] ⊂ ***Gst***CeuE and [Fe^{III}(**1**)Cp^*Ir^{III}] ⊂ ***Pth***CeuE) and the free catalyst ([Fe^{III}(**1**)Cp^*Ir^{III}]).

Detailed reaction protocol: 0.3 and 0.1 mM stock solutions of **4** and 0.3 and 0.6 mM stocks of **2** and **6** were prepared in catalytic buffer (0.6 M MES, 3 M HCOONa, pH 7). Triplicates of 200 μl were prepared in the concentration range from 0 to 0.3 mM (0, 0.01, 0.02, 0.03, 0.045, 0.07, 0.12, 0.21 and 0.3) or 0 to 0.6 mM (0, 0.03, 0.06, 0.09, 0.15, 0.30, 0.42, 0.54 and 0.6), diluting respective higher concentration stocks with catalytic buffer. For each set of reaction, one row of the 96-well plate was filled with 100 μl (each well) of 33 μM ArM or free catalyst (all prepared in 0.05 M Tris-HCl, 0.15 M NaCl, pH 7.5). The plate was then inserted into the plate reader and incubated for 5 min to equilibrate the temperature before starting the reaction. Measurements were undertaken of substrate-containing cells to prepare calibration curves. After 5 min, the plate was ejected and with the help of a multichannel pipetted, 20 μl of ArM or free catalyst were transferred from the respective wells to the substrate wells. The plate was reinserted into the instrument and kinetic measurements started immediately. All reactions were monitored for 2 h and measurements taken every 5 min. The formation or *(R)/(S)*-amines were determined using the calibration curves and the initial reaction rates (mM min^{-1}) determined by linear regression in the linear range. The kinetic parameters of the artificial enzymes were obtained by fitting the data to the standard Michaelis-Menten kinetic model, Origin Pro 2022b (Academic). Free catalyst data could not be successfully fitted using the model in the concentration range tested (**Fig. S1**).

4.4. Molecular docking

Molecular Docking was performed with [Fe^{III}(**1**)Cp^*Ir^{III}] ⊂ ***Cj***CeuE structure from PDB (id = 5OD5, assembly 3) and the three substrates: dihydroisoquinoline, harmaline and papaverine. The protein, cofactor and substrates were prepared with the Structure PrOtonation and REcognition System (SPORES) [32] with Protein-Ligand ANTSystem (PLANTS) [33] based on ant colony optimisation (where each component of the vector of variables that corresponds to one of the degrees of freedom of the protein or the ligand is in a function f, the optimisation algorithm then is to find a global minimum of this function). The interactions were visualised in ChimeraX (UCSF ChimeraX: Structure visualisation for researchers, educators, and developers) [34] and analysed by Maestro 2023 by Schrodinger.

Notes

The authors declare no competing financial interest.

CRediT authorship contribution statement

Alex H. Miller: Writing – original draft, Visualization, Validation, Methodology, Investigation, Formal analysis, Data curation, Conceptualization. **Ingrid B.S. Martins:** Methodology, Investigation, Formal analysis, Data curation. **Elena V. Blagova:** Investigation. **Keith S. Wilson:** Writing – review & editing, Funding acquisition, Conceptualization. **Anne-K. Duhme-Klair:** Writing – review & editing, Supervision, Funding acquisition, Data curation, Conceptualization.

Declaration of competing interest

The authors declare the following financial interests/personal relationships which may be considered as potential competing interests: Anne-K. Duhme-Klair reports financial support was provided by Engineering and Physical Sciences Research Council. Anne-K. Duhme-Klair reports financial support was provided by Biotechnology and Biological Sciences Research Council. Alex H. Miller reports financial support was provided by Engineering and Physical Sciences Research Council. Keith S. Wilson reports financial support was provided by Engineering and Physical Sciences Research Council. Elena V Blagova reports financial support was provided by Engineering and Physical Sciences Research Council. Keith S. Wilson reports financial support was provided by Biotechnology and Biological Sciences Research Council. Guest editor for Special Issue on Artificial Metalloenzymes. If there are other authors, they declare that they have no known competing financial interests or personal relationships that could have appeared to influence the work reported in this paper.

Data availability

Data will be made available on request.

Acknowledgment

We thank the UKRI Engineering and Physical Sciences Research Council (EPSRC grant reference EP/T007338/1) and the UKRI Biotechnology and Biological Sciences Research Council (BBSRC grant reference BB/W011131/1) for financial support.

ASSOCIATED CONTENT.

Appendix A. Supplementary data

Supplementary data to this article can be found online at https://doi.org/10.1016/j.jinorgbio.2024.112691.

References

[1] P. Dydio, H. Key, A. Nazarenko, J.-E. Rha, V. Seyedkazemi, D. Clark, J. Hartwig, Science 354 (2016) 102–106, https://doi.org/10.1126/science.aah4427.
[2] D.J. Raines, J.E. Clarke, E.V. Blagova, E.J. Dodson, K.S. Wilson, A.-K. Duhme-Klair, in: Nature Publishing Group (Ed.), Nature Catalysis vol. 1, 2018, pp. 680–688, https://doi.org/10.1038/s41929-018-0124-3.
[3] A.H. Miller, E.V. Blagova, B. Large, R.L. Booth, K.S. Wilson, A.-K. Duhme-Klair, ACS Catal. 14 (2024) 3218–3227, https://doi.org/10.1021/acscatal.3c05294.
[4] H.J. Davis, T.R. Ward, ACS Cent. Sci. 5 (2019) 1120–1136, https://doi.org/10.1021/acscentsci.9b00397.
[5] L. Alonso-Cotchico, J. Rodríguez-Guerra, A. Lledos, J.-D. Marechal, Acc. Chem. Res. 53 (2020) 896–905, https://doi.org/10.1021/acs.accounts.0c00031.
[6] U. Markel, D.F. Sauer, J. Schiffels, J. Okuda, U. Schwaneberg, Angew. Chem. Int. Ed. 58 (2019) 4454–4464, https://doi.org/10.1002/anie.201811042.
[7] M. Basle, H.A. Padley, F.L. Martins, G.S. Winkler, C.M. Jäger, A. Pordea, J. Inorg. Biochem. 220 (2021) 111446, https://doi.org/10.1016/j.jinorgbio.2021.111446.
[8] W.J. Song, J. Yu, F.A. Tezcan, J. Am. Chem. Soc. 139 (2017) 16772–16779, https://doi.org/10.1021/jacs.7b08981.
[9] L. Alonso-Cotchico, G. Sciortino, P. Vidossich, J. Rodríguez-Guerra Pedregal, I. Drienovská, G. Roelfes, A. Lledós, J.-D. Maréchal, ACS Catal. 9 (2019) 4616–4626, https://doi.org/10.1021/acscatal.8b04919.
[10] E.V. Blagova, A.H. Miller, M. Bennett, R.L. Booth, E.J. Dodson, A.-K. Duhme-Klair, K.S. Wilson, Acta Crystallogr. Sect. D 79 (2023) 694–705, https://doi.org/10.1107/S2059798323004473.
[11] M. Jeschek, R. Reuter, T. Heinisch, C. Trindler, J. Klehr, S. Panke, T.R. Ward, Nature 537 (2016) 661–665, https://doi.org/10.1038/nature19114.
[12] K. Oohora, T. Hayashi, Dalton Trans. 50 (2021) 1940–1949, https://doi.org/10.1039/D0DT03597A.
[13] S. Tang, L.-J. Sun, A.-Q. Pan, J. Huang, H. Wang, Y.-W. Lin, Org. Biomol. Chem. 21 (2023) 9603–9609, https://doi.org/10.1039/D3OB01687K.
[14] L.-J. Sun, H. Yuan, J.-K. Xu, J. Luo, J.-J. Lang, G.-B. Wen, X. Tan, Y.-W. Lin, Biochemistry 62 (2021) 369–377, https://doi.org/10.1021/acs.biochem.1c00554.
[15] A.H. Miller, S.A. Thompson, E.V. Blagova, K.S. Wilson, G. Grogan, A.-K. Duhme-Klair, Chem. Commun. 60 (2024) 5490–5493, https://doi.org/10.1039/D4CC01158A.
[16] K.J. Koebke, T.B. Pinter, W.C. Pitts, V.L. Pecoraro, Chem. Rev. 122 (2022) 12046–12109, https://doi.org/10.1021/acs.chemrev.1c01025.
[17] D.J. DiPrimio, P.L. Holland, J. Inorg. Biochem. 219 (2021) 111430, https://doi.org/10.1016/j.jinorgbio.2021.111430.
[18] F. Yu, V.M. Cangelosi, M.L. Zastrow, M. Tegoni, J.S. Plegaria, A.G. Tebo, C. S. Mocny, L. Ruckthong, H. Qayyum, V.L. Pecoraro, Chem. Rev. 114 (2014) 3495–3578, https://doi.org/10.1021/cr400458x.
[19] S.D. Khare, Y. Kipnis, P.J. Greisen, R. Takeuchi, Y. Ashani, M. Goldsmith, Y. Song, J.L. Gallaher, I. Silman, H. Leader, Nat. Chem. Biol. 8 (2012) 294–300, https://doi.org/10.1038/nchembio.777.
[20] L. Marchetti, M. Levine, ACS Catal. 1 (2011) 1090–1118, https://doi.org/10.1021/cs200171u.
[21] S. Hirota, Y.-W. Lin, JBIC J. Biol. Inorg. Chem. 23 (2018) 7–25, https://doi.org/10.1007/s00775-017-1506-8.
[22] J. Zhang, D. Liao, R. Chen, F. Zhu, Y. Ma, L. Gao, G. Qu, C. Cui, Z. Sun, X. Lei, Angew. Chem. 134 (2022) e202201908, https://doi.org/10.1002/anie.202201908.
[23] N.V. Igareta, R. Tachibana, D.C. Spiess, R.L. Peterson, T.R. Ward, Faraday Discuss. (2023), https://doi.org/10.1039/D3FD00034F.
[24] V.M. Robles, M. Dürrenberger, T. Heinisch, A. Lledos, T. Schirmer, T.R. Ward, J.-D. Marechal, J. Am. Chem. Soc. 136 (2014) 15676–15683, https://doi.org/10.1021/ja508258t.
[25] F. Schwizer, V. Köhler, M. Dürrenberger, L. Knörr, T.R. Ward, ACS Catal. 3 (2013) 1752–1755, https://doi.org/10.1021/cs400428r.
[26] K. Kariyawasam, T. Di Meo, F. Hammerer, M. Valerio-Lepiniec, G. Sciortino, J. D. Maréchal, P. Minard, J.P. Mahy, A. Urvoas, R. Ricoux, Chemistry–A European J 26 (2020) 14929–14937, https://doi.org/10.1002/chem.202002434.
[27] R. López-Domene, A. Manteca, A. Rodriguez-Abetxuko, A. Beloqui, A. L. Cortajarena, Chem Eur J (2024) e202303254, https://doi.org/10.1002/chem.202303254.
[28] N.T. Nguyen, T.H. Nguyen, T.N.H. Pham, N.T. Huy, M.V. Bay, M.Q. Pham, P. C. Nam, V.V. Vu, S.T. Ngo, J. Chem. Inf. Model. 60 (2019) 204–211, https://doi.org/10.1021/acs.jcim.9b00778.
[29] C. Marchi-Delapierre, L. Rondot, C. Cavazza, S. Menage, Isr. J. Chem. 55 (2015) 61–75, https://doi.org/10.1002/ijch.201400110.
[30] Y. Yu, A. Rué Casamajo, W. Finnigan, C. Schnepel, R. Barker, C. Morrill, R.S. Heath, L. De Maria, N.J. Turner, N.S. Scrutton, ACS Catal. 13 (2023) 12310–12321, https://doi.org/10.1021/acscatal.3c02278.
[31] C. Boss, C. Brisbare-Roch, F. Jenck, M. Steiner, European Patent Office, Actelion Pharmaceuticals Ltd (2010). EP2402322A1: https://patents.google.com/patent/EP2402322A1/en.
[32] T. ten Brink, T.E. Exner, J. Chem. Inf. Model. 49 (2009) 1535–1546, https://doi.org/10.1021/ci800420z.
[33] O. Korb, T. Stützle, T.E. Exner, Swarm Intelligence 1 (2007) 115–134, https://doi.org/10.1007/s11721-007-0006-9.
[34] E.F. Pettersen, T.D. Goddard, C.C. Huang, E.C. Meng, G.S. Couch, T.I. Croll, J. H. Morris, T.E. Ferrin, Protein Sci. 30 (2021) 70–82, https://doi.org/10.1002/pro.3943.